Ph. Boland & F. Janssens
Mathematical Division, ESTEC, Noordwijk, The Netherlands

The Geos-1 Dynamic Experiment

Abstract The nonlinearity of the Euler equations implies that a spinning satellite may be despun quite rapidly when subjected to continuous axial thrusting. This phenomenon and the conditions under which it occurs are discussed here. The problem has been recognised with a multibody computer program simulating the complete equations of motion. An approximate expression for average spin evolution is derived for a spinning spacecraft with two radial wire appendages. Because of the importance of the phenomenon for such future projects as the International Solar-Polar Mission (ISPM), an in-flight verification has been made using the Agency's Geos-1 scientific satellite. The agreement between the theoretical predictions and the in-flight data has proved to be excellent.

Résumé Pour un satellite en rotation, la non-linéarité des équations d'Euler fait que la rotation peut être freinée rapidement sous l'influence d'une poussée axiale continue. Ce phénomène et les conditions de son apparition font l'objet du présent article. On a procédé à une analyse du problème au moyen d'un logiciel permettant de simuler intégralement les équations du mouvement en tenant compte des attractions exercées par les différents corps célestes en présence. On obtient une expression approchée de l'évolution moyenne de la rotation d'un satellite équipé de deux appendices constitués par des câbles radiaux. Vu l'importance du phénomène pour certains projets futurs telle que la Mission internationale d'étude des régions polaires du Soleil (ISPM), on a procédé à une vérification en vol sur le satellite scientifique Geos-1 de l'ESA. Les résultats obtenus à cette occasion sont en excellent accord avec la théorie.

Introduction

The loss of Explorer-I in 1958 was the first unpleasant surprise with spin-stabilised spacecraft, but it was not the last; a number of other examples of unexpected in-flight behaviour are quoted in Reference 1. The two recurring problem areas in these examples are the interactions between the control system and certain flexible elements of the spacecraft (Mariner-10, ATS-V), and neglected nonlinearities in the dynamical model (Tacsat). Most of these sagas have had happy endings and have stressed the importance of the art of modelling. This article describes another example of a nonlinear effect that may cause rapid despinning and subsequent loss of a spacecraft.

The potential victim was Geos-1, a scientific magnetospheric-explorer satellite (launched on 20 April 1977), which spins nominally at 10 rpm about its axis of maximal inertia and carries two 20 m-long radial wire booms or cables. An orbit manoeuvre with continuous axial thrusting was planned for Geos in May 1979, a similar manoeuvre having already been executed on 26 April 1977, shortly after apogee-boost-motor firing (booms in stowed configuration). This first manoeuvre lasted three minutes and was nominal in the sense that only a spin down from 96 to 95 rpm was noted. As the new orbit manoeuvre was to take place with the booms fully deployed, there was some concern about their behaviour.

From inspection of the linearised equations of motion one would only conclude that the manoeuvre is safe. As a systematic check, however, a computer simulation based on the full (nonlinear) equations of motion in a multibody formulation[2] was performed. The results predicted complete despin and subsequent loss of the satellite due to slackness in the wire cables in just a few minutes[3]. Intensive program checking confirmed the consistency of the results. At the same time, a closer look at the full Euler equations for a rigid body indicated the possibility of a similar type of behaviour.

With this level of understanding of the phenomenon it was decided to execute the planned orbit manoeuvre using a radial thruster in pulsed mode instead of an axial thruster in continuous mode. This changed the manoeuvre duration from 45 min to 9 h. According to Reference 2, the spin variations associated with this type of thrusting are negligible.

An in-flight verification of these predictions was later proposed by the dynamics group in view of the potential importance of the phenomenon. The ISPM project group supported this verification, because a similar situation could occur during an ISPM spacecraft mid-course correction manoeuvre if one of the axial thrusters were to fail.

The verification manoeuvre was conducted in two segments from the Agency's European Space Operations Centre (ESOC) in Darmstadt (Germany), on the 27 and 28 September 1979[4].

A direct comparison between the outputs of the Geos satellite's on-board accelerometers and the theoretical predictions is presented in this paper. The correlation between telemetry data and simulation is convincing, especially for the variations in spin rate.

The nonlinear effects discussed here are little known and not explicitly discussed in the literature, although the phenomenon of interest is a special case of the self-excited rigid body[5,6]. The crucial point is the thruster location with respect to the principal axes of inertia of the satellite. The underlying theory for a rigid body and the extension to a central body with two cable booms appended is provided in the last section. An approximate expression is derived to calculate the time to complete despin. The results show that the destabilisation time is inversely proportional to the third power of the initial spin rate. In this respect, the success of the first orbital manoeuvre conducted with Geos's booms stowed was due to the very high spin at that stage of the mission, rather than to the fact that the cable booms had yet to be deployed.

The in-flight experiment

System modelling

Despite the many flexible booms and antennas that surround the main body of the Geos satellite (Fig. 1), the overall dynamic response of the system can be

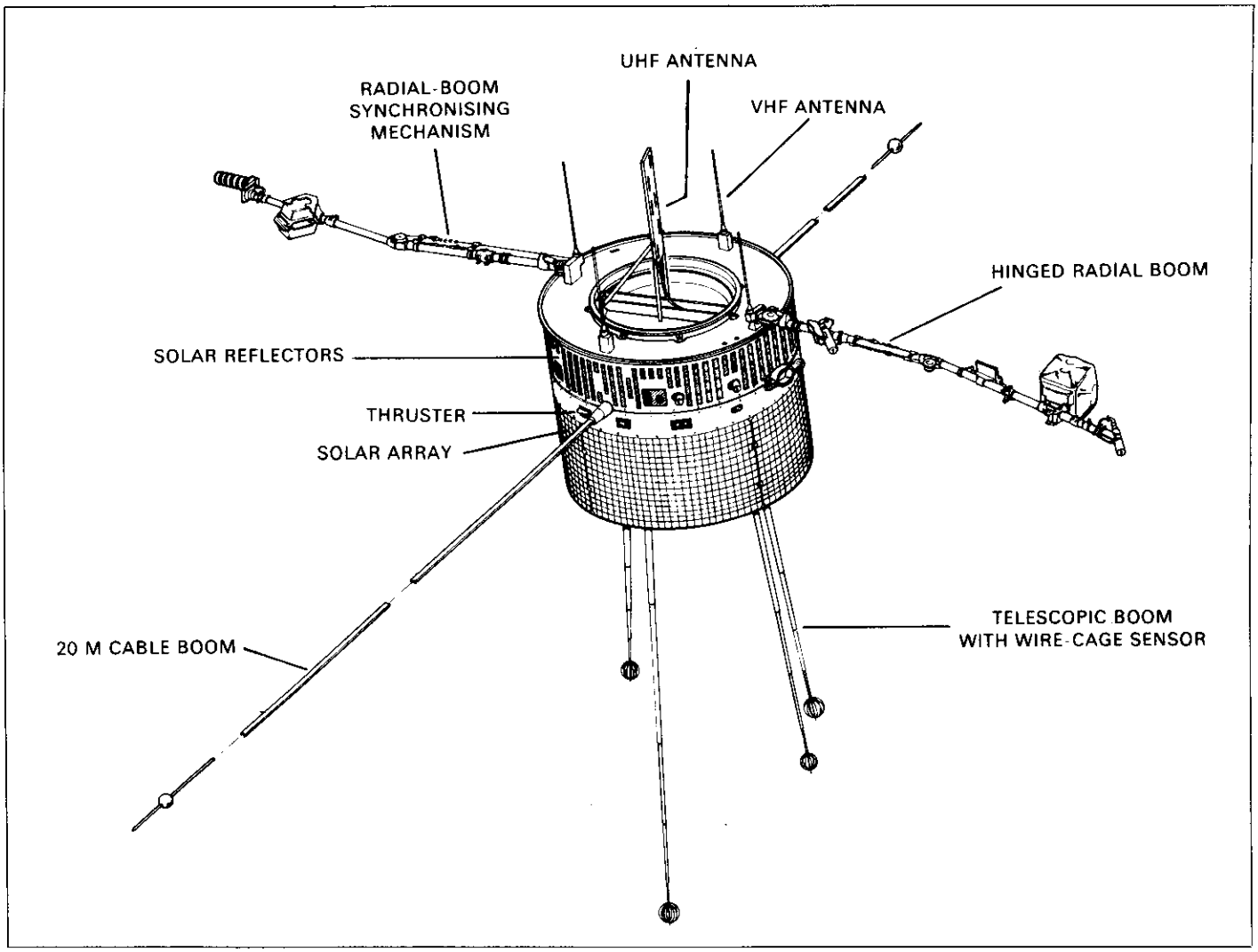

Figure 1

simulated satisfactorily by a simple model including one rigid body and two hinged bars to represent the 20 m cable booms, the remaining appendages being considered as rigid. The bars are assigned the same mass and inertia characteristics as the corresponding flexible elements. Detailed analysis shows in fact that the deformation modes for which the cables depart substantially from a straight line can be ignored. The connections between the central body and the cable booms are represented by two-degree-of-freedom joints, so that the resulting relative motions can be broken down into oscillations in one plane perpendicular to the spin axis (equatorial plane), and another containing that axis (meridian plane). No damping is represented, although Geos is equipped with a particularly effective nutation damper and root dampers for the cable booms. This omission has no major consequences as far as the dynamical phenomenon of interest is concerned, namely the spin variations associated with the action of an axial external force on the satellite.

The pre-flight simulation of the planned test manoeuvre was made with a generic, discrete-coordinate simulation program. This digital computer program has the capacity to simulate the large-angle motion (nonlinear equations) response of interconnected rigid-body systems to external forces, with possible constraints for the interbody connections. The program is currently being used for preliminary studies of the attitude dynamics and appendage-deployment phases of spacecraft with flexible appendages. Such investigations may have a considerable impact on manoeuvre strategies (the subject of this paper being a dramatic example), mechanical design and control-system definition.

Pre-flight simulations

We shall now analyse qualitatively the dynamic behaviour of Geos as predicted

Table 1. Input data in reference frame (Fig. 2)

Main body	
Mass (kg)	: 273.68 (including 4 kg of fuel)
Height of CG above separation plane (m)	: 0.502
Inertias along X, Y, Z (kgm^2)	: 78.37, 163.51, 170.98
Cable booms	
Root location (m)	: (0, ±1.101, −0.1797)
Specific mass (kg·m)	: 0.0224
Length (m)	: 19.75
Tip mass (kg)	: 0.1072
Lower axial thruster	
Location (m)	: (0.555, 0.466, −0.394)
Direction	: (0, 0, 1)
Level (N)	: 7
Mode	: continuous
Inclined accelerometer	
Location (m)	: (−0.6925, 0, 0.2763)
Sensitive direction	: (0, 0.7071, −0.7071)
Vertical accelerometer	
Location (m)	: (0, −0.6925, 0.3731)
Sensitive direction	: (0, 0, 1)

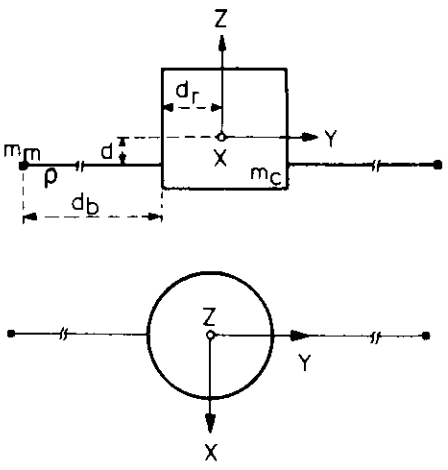

Figure 2

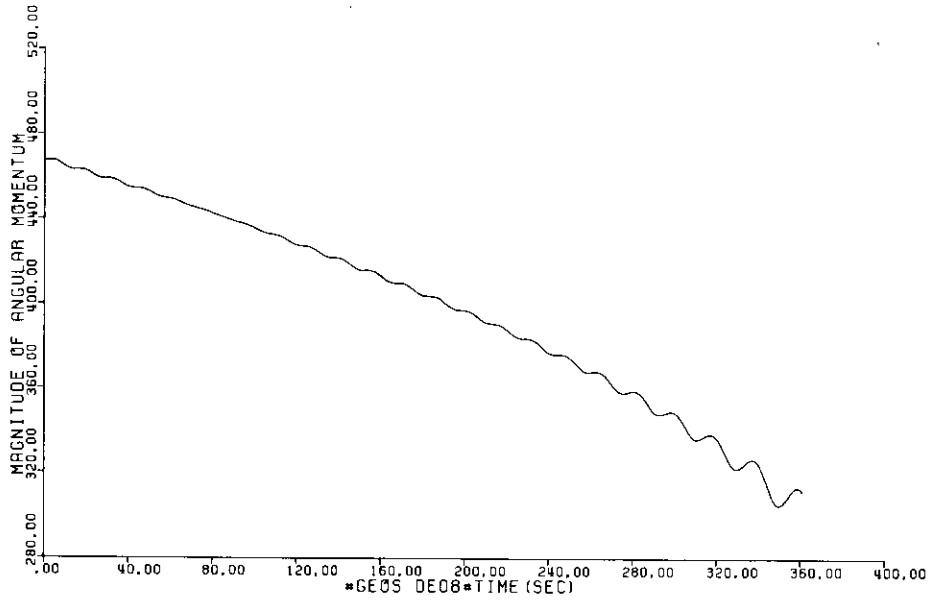

Figure 3

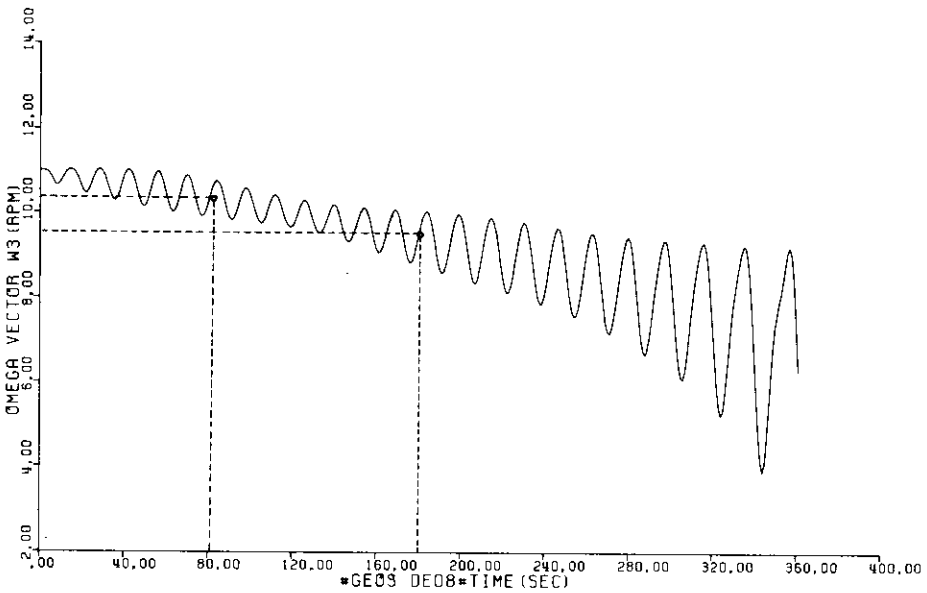

Figure 4

by computer simulation when the lower axial thruster is operated in continuous mode. The basis of the mathematical model is shown in Figure 2. The satellite's mass and configuration at the time of the dynamic experiment are summarised in Table 1, the frame of reference being centred on the main body's centre of mass, with the orientation indicated in Figure 2.

Let us concentrate first on the variations in the system's total angular momentum. The axial force fixed in the main body generates a spinning torque which is perpendicular to the angular momentum when the excitation starts. As one may anticipate intuitively, a unit vector aligned with the angular-momentum vector will describe a cone in inertial space, at spin frequency. In the present case the corresponding cone half-angle remains smaller than 1°. Of more interest is the time history of the magnitude of the angular momentum, which undergoes a systematic deviation from its nominal value, as illustrated in Figure 3. If the action of the external torque is stopped at some particular instant, the angular momentum will remain constant and the satellite will reacquire its equilibrium configuration after the system oscillations have damped out. The resulting spin rate is then easily calculated as the ratio between the magnitude of the angular momentum and the spin inertia of the system. From this we can conclude that the satellite's instantaneous mean spin rate must vary in much the same way; this is confirmed in Figure 4, where the third component of the omega vector is plotted as a function of time.

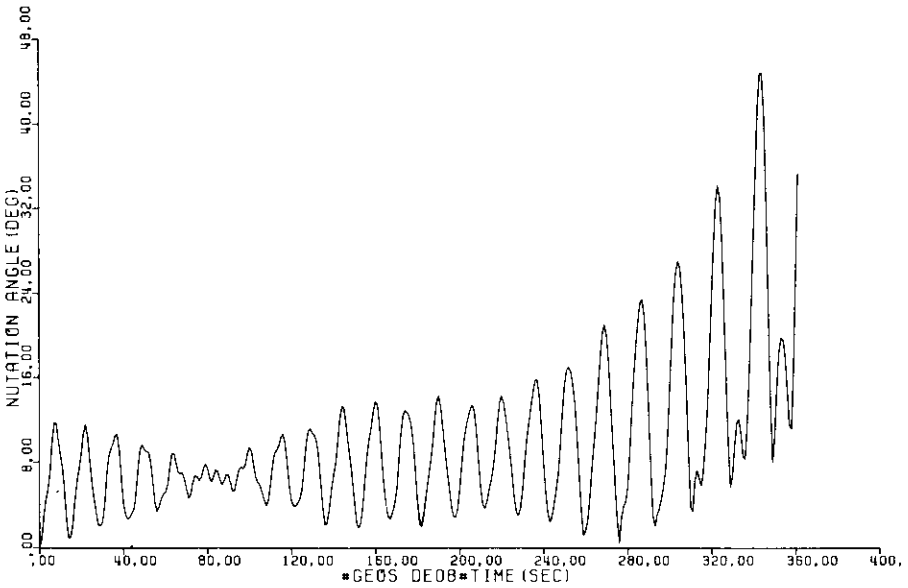

Figure 5

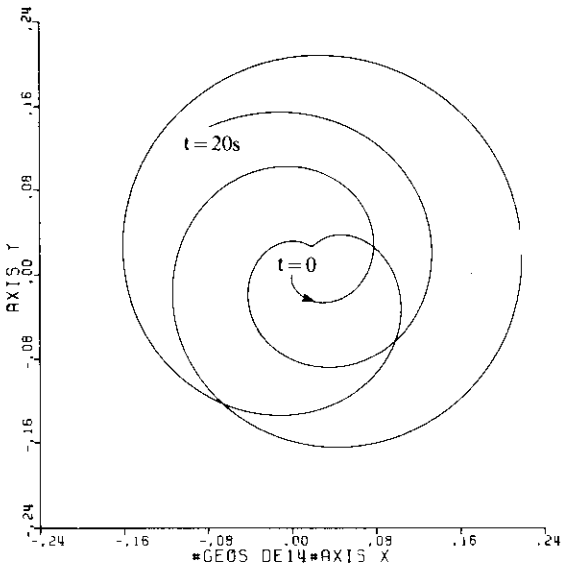

Figure 6

It is worth noting that such dynamic behaviour is not predictable on the basis of linearised equations of motion. Linear analysis shows, on the contrary, that the spin rate should be constant during such excitation[7]. The despin phenomenon must, therefore, be attributed to nonlinear effects. This is deduced on an analytical basis in the next section. A sound understanding of the problem can, however, be gained by considering the spacecraft motions, as explained below.

When the continuous axial force is applied, the body-fixed Z-axis (Fig. 2) begins to wander about the angular momentum vector. The nutation angle (measured between these two directions) is plotted against time in Figure 5. The resulting oscillations are at the nutation frequency for this type of excitation, whereas twice this frequency is always associated with the nutation-angle variation when the motion is force-free. The nutation frequency is a characteristic frequency of the system and is identified from modal-analysis considerations.

The motion of the centre body in inertial space can be visualised by examining the trace of the body-fixed Z-axis on a plane fixed in inertial space. This is shown in Figure 6, where the plane of reference is perpendicular to the body Z-axis when the manoeuvre is initiated.

From the comments above it is clear that the body-fixed torque vector corresponding to the applied force and the angular-momentum vector do not remain perpendicular to each other, due to nutation. The work produced by this continuous torque therefore varies periodically at the nutation frequency. From

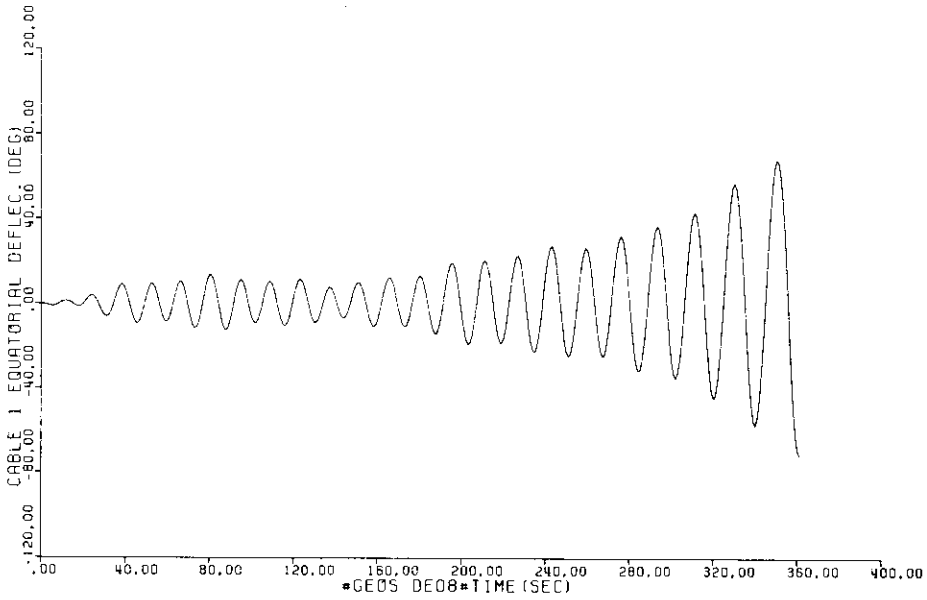

Figure 7

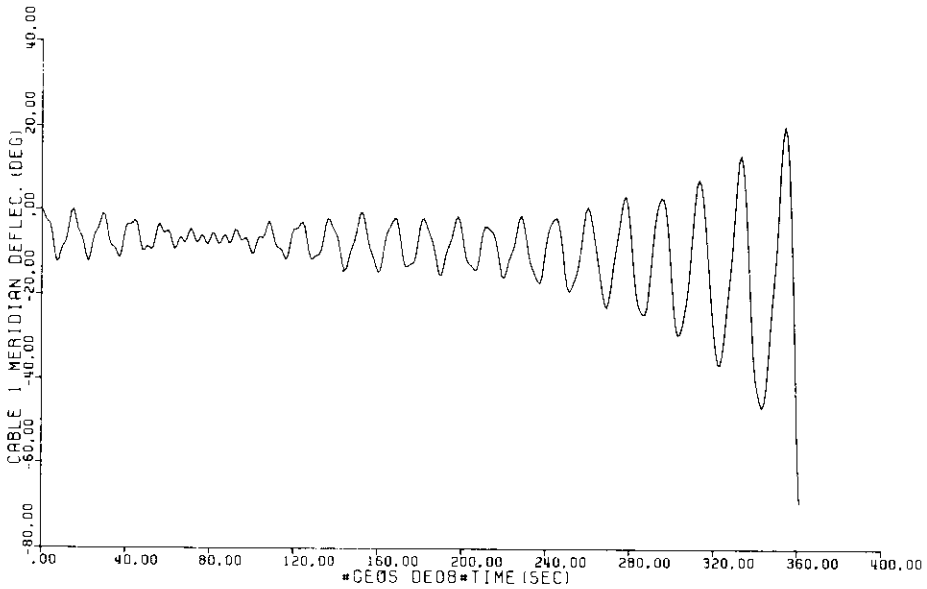

Figure 8

this it can easily be conceived that the mean value of this function over a nutation period does not necessarily average to zero, but rather depends on geometric characteristics of the system. The conditions that govern the variations in the angular momentum are established in the final section of this paper.

It should be clear from the preceding arguments that the spin variations are forced at nutation frequency (Fig. 4). The cable booms are in turn forced into antisymmetric oscillations in the equatorial plane at the same frequency. The relative angular displacements of one cable in the equatorial plane with respect to the centre body is shown in Figure 7. As outlined previously, this is a nonlinear response to the type of perturbation under consideration, since the eigenfrequency of the system which characterises this type of cable boom motion is basically different for this length of cables.

Turning our attention now to the oscillations of the cables in the meridian plane, we can see by simple examination that the traces of Figures 5 and 8 are similar but of opposite sign. This is typical of the so-called 'nutation mode' of this mechanical system, which can be identified from linear equations[7]. The cables experience antisymmetric displacements for this mode, which is always coupled with a higher frequency but otherwise similar mode, the so-called 'meridian antisymmetric mode'. This high-frequency vibration is clearly present in Figures 5 and 8.

Another characteristic of Figures 4, 5, 7 and 8 is the modulation in amplitude of

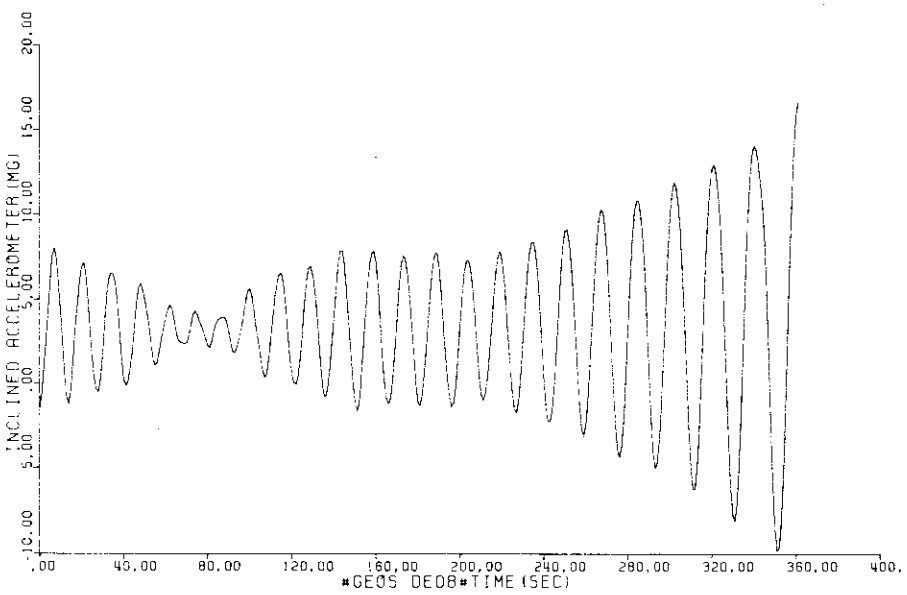

Figure 9

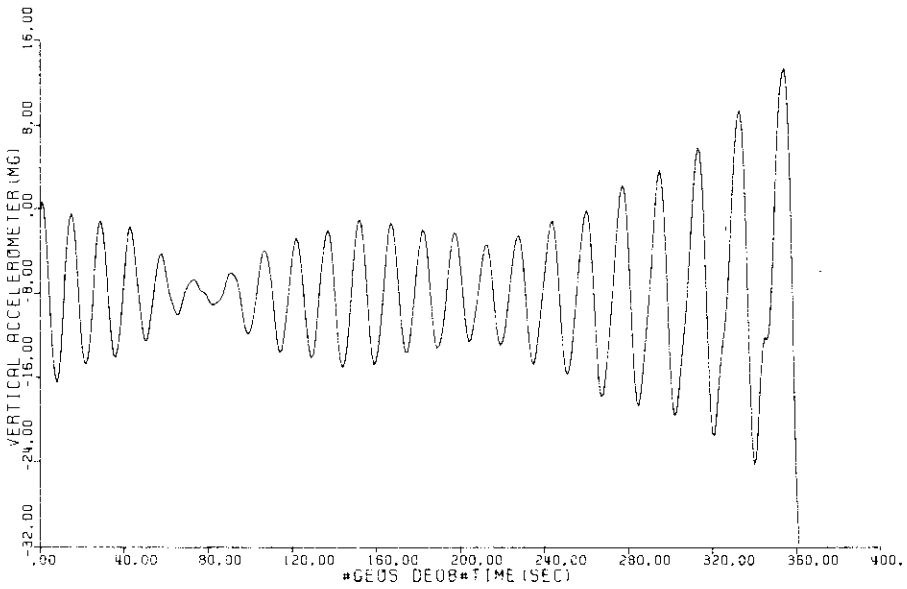

Figure 10

the corresponding signals. The periods of modulation can be obtained by introducing the spin-rate variations at nutation frequency into the linearised equations of motion. This changes the linear equations with constant coefficients into linear equations with periodic coefficients. The observed modulations can then be explained in terms of parametric excitations.

To summarise, the general dynamic behaviour of Geos under continuous axial thrusting conditions is governed essentially by the nonlinear part of the equations of motion, although some system modes typical of linear response are also present. The long-term effect of the resulting torque is a despinning of the spacecraft and a consecutive build-up of nutational motion, as illustrated in Figure 5, the cable booms making wild oscillations at the same time (Figs. 7 & 8). It should be noted that the cables themselves could become slack long before that moment.

Determination of manoeuvre parameters

To establish the validity of the theoretical predictions that led to the changing of the strategy for the orbital manoeuvre planned for May 1979, it was desirable to devise the experiment manoeuvre so as to produce a significant spin-rate reduction, thereby causing a sensible increase in the nutational motion. This requirement had to be compatible with the many system and operational constraints[4]; there are stringent conditions on the minimum spin rate (7.5 rpm) to ensure proper functioning of the attitude-measurement system, and on the

maximum nutation angle (15°) to maintain a good-quality radio link with the ground stations.

In view of the above, and taking into account the fact that some of the system parameters, such as thrust level and residual fuel were not accurately known, extensive computer-simulation runs were made to cover a wide range of system parameters. As indicated in Reference 3, the optimal strategy turned out to be a 3 min manoeuvre with an initial spin rate of 11 rpm. This would allow the predictions to be confirmed with reasonable margins with respect to the system constraints.

Monitoring of the manoeuvre

The dynamic behaviour of the Geos satellite is monitored mainly by the pair of on-board accelerometers, the exact locations of which are given in Table 1, their sensing directions being parallel (vertical accelerometer) and inclined by 45° (inclined accelerometer) to the body-fixed Z-axis. The corresponding telemetry output is plotted in real time on strip-chart recorders in the Control Room at (ESOC). This provides immediate insight into spacecraft behaviour and, at the same time, a valuable base for real-time decision making during a manoeuvre. The computer-simulated accelerometer traces corresponding to Figures 3-8 are reproduced in Figures 9 and 10.

Spin rate is measured via the satellite's optical sensor system, which is designed to provide only one type of measurement every 45 s. In this respect it was not possible to assess the mean spin rate until well after the manoeuvre had been completed; neither was it possible to monitor the constantly changing attitude of the spacecraft during the manoeuvre with the set of solar and earth sensors.

Comparison of predictions and telemetry data

Since the experiment was somewhat critical in terms of spacecraft security, it was decided to make a preliminary excitation manoeuvre lasting 80 s, to check proper functioning of the subsystems and to evaluate the correspondence between predictions and flight behaviour. This first manoeuvre segment was followed by the 3 min experiment the next day. The satellite's spin rate was adjusted to the requisite value before each manoeuvre by tangential thrusting.

Table 2 compares the spin variations obtained by computer simulation and those measured on-board the satellite; the excellent agreement is readily apparent. The corresponding points are indicated in Figure 4.

Table 2

Manoeuvre duration (s)	Initial spin (rpm)	Final spin (rpm)	
		predicted	measured
82	10.97	10.36	10.36
181	11.00	9.50	9.53

Telemetry data were used to produce the plots of Figures 11 and 12, corresponding to the first and second manoeuvres. A direct comparison is shown with the computer-simulated outputs, which had been scaled to the format of the strip-chart recorders. The accelerations are measured in milli-g's as a function of time in seconds. The saturation level at ± 12.5 mg has been included in the predictions.

The acceleration at any point in the main body depends on all of the system parameters. Any deficiency in the system modelling may therefore affect the resemblance between the simulated and actual time histories of these accelerations. Nevertheless, Figures 11 and 12 show good agreement between predictions and real-time telemetry data for the on-board accelerometer outputs.

The differences in magnitude which can be observed are attributed to damping, which was not incorporated in the mathematical modelling. In this respect, the

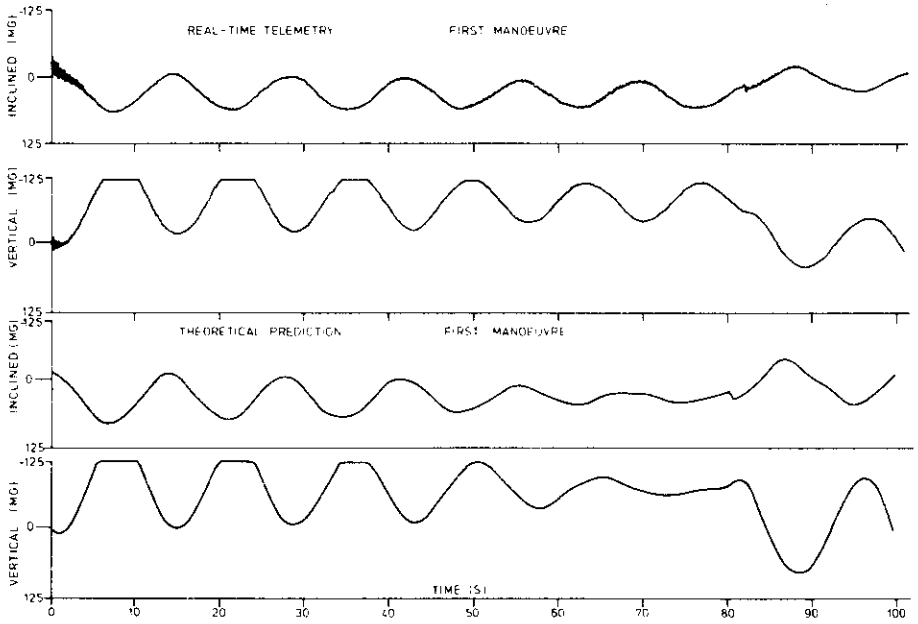

Figure 11

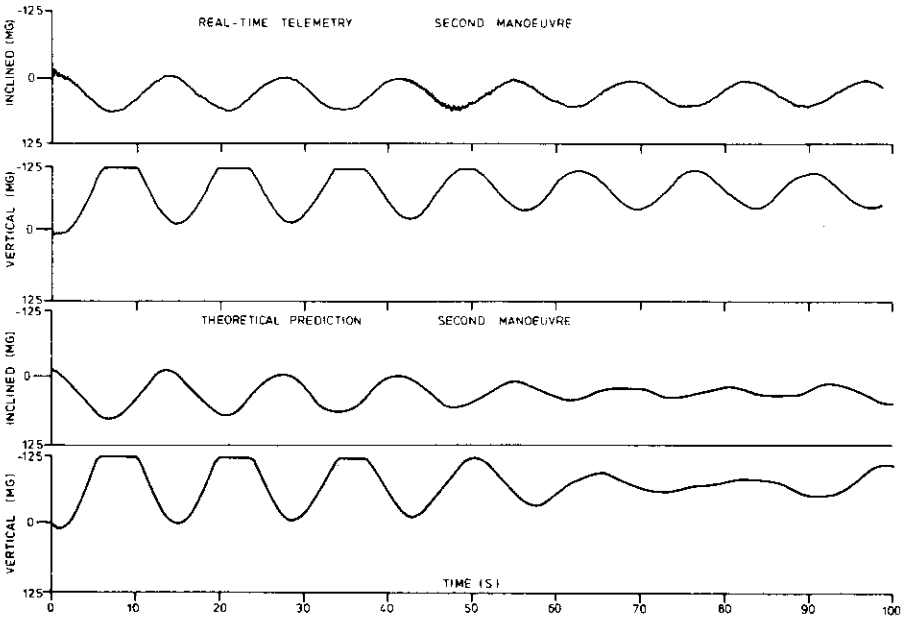

Figure 12a

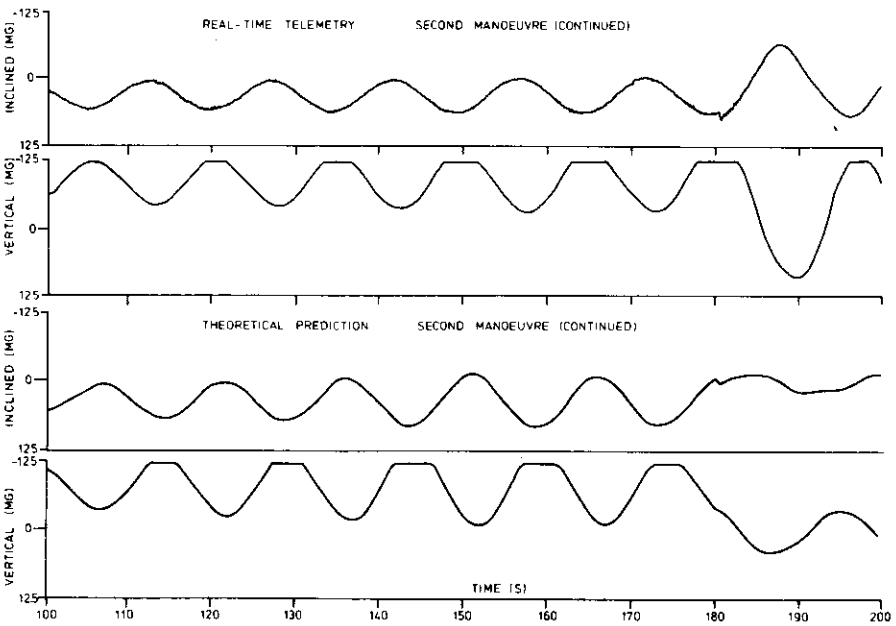

Figure 12b

amplitude modulation of these signals is much less pronounced for the actual data, although it is still quite visible. The predictions show a shift in the phase of the accelerometer signals as a result of the narrowing associated with the amplitude modulation. This phenomenon is not reproduced in the actual accelerometer outputs. As a direct consequence, the amplitudes of accelerations corresponding to the consecutive free motions are different. This is particularly apparent for the second manoeuvre.

Averaged spin evolution via linearised equations

A rigid body spinning uniformly around its major axis of inertia is subjected to continuous axial thrusting from time t_0 onwards. The equivalent force, antiparallel to the absolute exhaust velocity, is considered as axial. The thruster is not located on the spin axis, so that a body-fixed constant equatorial torque is applied to the spinner. The mass variation due to fuel consumption is neglected.

This problem is a special case of the self-excited rigid body as defined in Reference 6 (pp. 145-153) and References 8 and 9. A complete analytical solution is not available although the self-excited rigid body is the simplest generalisation possible from the force-free case, as the right-hand sides of the Euler equations are arbitrary constants instead of zeros. The 'self-excited rigid body' represents a problem of considerable practical interest, as it also describes flat-spin recovery procedures[10].

Under the assumptions mentioned, one would intuitively expect the effect of the equatorial torque on the energy and angular momentum to average out over one revolution, and that consequently these quantities cannot change significantly. It will be shown here that this expectation is not always confirmed.

Rigid body

The Euler equations for the problem considered are:

$$\begin{aligned} A\dot{\omega}_1 + (C-B)\omega_2\omega_3 &= t_1 \\ B\dot{\omega}_2 + (A-C)\omega_3\omega_1 &= t_2 \\ C\dot{\omega}_3 + (B-A)\omega_1\omega_2 &= 0 \\ A < B < C & \end{aligned} \tag{1}$$

The initial conditions are:

$$\omega_1(0) = \omega_2(0) = 0 \qquad \omega_3(0) = \Omega > 0$$

Linearising about the initial conditions changes Equation (1) into

$$\begin{aligned} A\dot{\omega}_1 + (C-B)\Omega\omega_2 &= t_1 \\ B\dot{\omega}_2 - (C-A)\Omega\omega_1 &= t_2 \\ \omega_3 &= \Omega \end{aligned} \tag{2}$$

The solution of Equation (2) will be discussed in some detail to establish for how long it is valid and what type of evolution takes place. This solution is easily obtained as

$$\omega_1(t) = \frac{t_1}{A\Omega N}\sin\Omega Nt - \frac{t_2}{(C-A)\Omega}(1-\cos\Omega Nt)$$

$$\omega_2(t) = \frac{t_2}{B\Omega N}\sin\Omega Nt + \frac{t_1}{(C-B)\Omega}(1-\cos\Omega Nt) \tag{3}$$

with $N^2 = \dfrac{(C-A)(C-B)}{AB}$

To examine the displacement of the rotation vector ω in the body, we write Equation (3) as

$$\omega_1 - \bar{\omega}_1 = \frac{A_m}{\Omega\sqrt{(C-A)A}} \cos(\Omega N t - \varphi_1)$$

$$\omega_2 - \bar{\omega}_2 = \frac{A_m}{\Omega\sqrt{(C-B)B}} \sin(\Omega N t - \varphi_1) \tag{4}$$

where

$$\bar{\omega}_1 = \frac{-t_2}{(C-A)\Omega} \qquad \bar{\omega}_2 = \frac{t_1}{(C-B)\Omega} \tag{5}$$

$$A_m^2 = \frac{B}{C-B} t_1^2 + \frac{A}{C-A} t_2^2 \qquad \tan\varphi_1 = \frac{t_1}{t_2}\sqrt{\frac{C-A}{C-B}\frac{B}{A}} \tag{6}$$

Equation (4) is the parametric equation of ellipses, such as are given in Figure 13.

These trajectories have the following notable properties:

- The centre M has coordinates $(\bar{\omega}_1, \bar{\omega}_2)$; its direction is independent of Ω.
- The principal axes of the ellipses are always parallel to the principal axes of the rigid body. The semi-major axis is parallel to the intermediate axis of inertia and the semi-minor axis to the minimal axis for any value of the applied torque $T(t_1, t_2)$.
- The eccentricity of these ellipses is independent of the applied torque and the spin rate; it is a function of the inertias only.

$$e^2 = 1 - \frac{(C-B)B}{(C-A)A} = \frac{(B-A)(A+B-C)}{A(C-A)} \tag{7}$$

- The nutation frequency ΩN defines the uniform time evolution of the eccentric anomaly. This type of time dependency implies that the two equal parts of the ellipse obtained by the division by an arbitrary diameter are completed in half a period.
- The velocity v of the rotation vector ω varies between

$$\sqrt{\frac{C-B}{B(C-A)}}\frac{A_m}{A} \leq v \leq \sqrt{\frac{C-A}{A(C-B)}}\frac{A_m}{B}$$

- The maximum is reached at the crossing of the semi-major axes.
- The maximal deviation of the rotation vector from its initial direction occurs at the points D (Fig. 13). As this direction does not pass through the centre M, the evolution of this duration from D to O cannot be the symmetric part of that from O to D.
- From the scalar product $< M, T >$ one can distinguish the following cases for the angle between these two directions:

$$< M, T > = \frac{t_1 t_2}{\Omega} \frac{B-A}{(C-A)(C-B)} \tag{8}$$

$$t_1 \cdot t_2 > 0 \rightarrow \text{angle } M, T < \frac{\pi}{2}$$

$$t_1 \cdot t_2 < 0 \rightarrow \text{angle } M, T > \frac{\pi}{2}$$

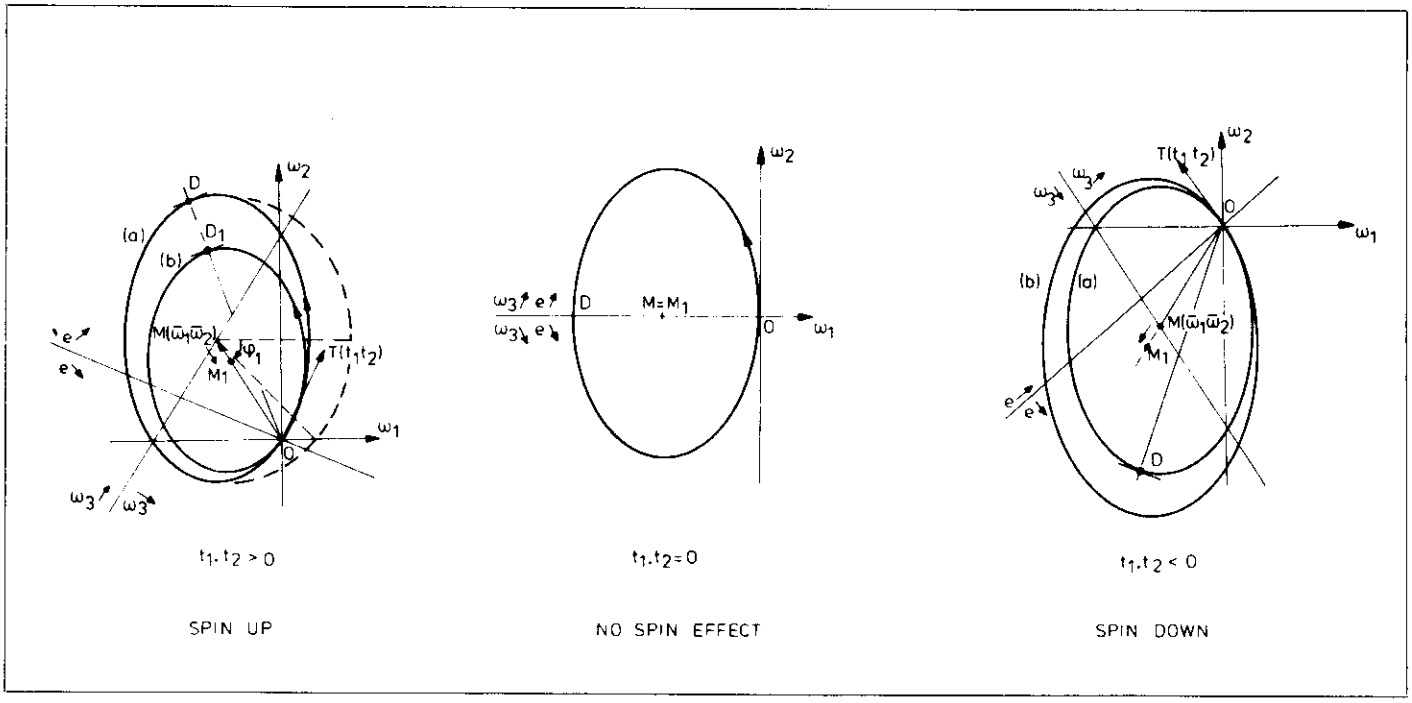

Figure 13

The ω_1, ω_2 axes are aligned with the two equatorial principal axes:

ω_1: parallel to the principal axis of minimal inertia

ω_2: parallel to the principal axis of intermediate inertia

During the first nutation period, the ellipse (a) with centre M is described. During the second nutation period, the ellipse (b) with centre M_1 is described.

This last property is important when discussing the evolution of the energy and h, which is half of the square of the module of the angular momentum. The rate of change of these quantities is easily obtained from Equation (1):

$$\dot{e} \equiv \frac{1}{2}\frac{d}{dt}(A\omega_1^2 + B\omega_2^2 + C\omega_3^2) = \omega_1 t_1 + \omega_2 t_2 \tag{9}$$

$$\dot{h} \equiv \frac{1}{2}\frac{d}{dt}(A^2\omega_1^2 + B^2\omega_2^2 + C^2\omega_3^2) = A\omega_1 t_1 + B\omega_2 t_2 \tag{10}$$

$\dot{e}$ and $\dot{h}$ are simply the scalar products of the applied torque with the ω and h vectors, respectively.

The ellipses of Figure 13 are divided into two unequal parts by the perpendicular to T. One part defines the zone where the energy is increased $\dot{e} = <\omega, T> > 0$ whereas the other part corresponds to a reduction in the energy. As more time is spent in the zone that contains the centre one can expect a resultant net increase or decrease in the energy depending on the position of M.

These considerations are valid as long as the ω trajectory can be used as a reference or as long as the change in energy per revolution is small (period $T = 2\pi/\Omega N$). The averaged changes in e and h are then approximated by

$$\bar{\dot{e}} = \frac{1}{T}\int_0^T \dot{e}\,dt \tag{11}$$

$$\bar{\dot{h}} = \frac{1}{T}\int_0^T \dot{h}\,dt \tag{12}$$

Substituting Equations (3), (9) and (10) in Equations (11) and (12), only the constant terms will remain and

$$\bar{\dot{e}} = \frac{t_1 t_2}{\Omega}\frac{B-A}{\sqrt{(C-A)(C-B)}} \tag{13}$$

$$\bar{\dot{h}} = \frac{t_1 t_2}{\Omega} C \frac{B-A}{\sqrt{(C-A)(C-B)}} \tag{14}$$

These two equations provide the following information:

- If t_1 or $t_2 = 0$ or B = A (symmetric body), e and h remain constant on the average. No secular effects on spin rate are present and Equation (3) always represents a good approximation to the exact solution, which can be found in Reference 6.
- If t_1 and $t_2 = 0$, the averaged energy $\tilde{e}$ and averaged $\tilde{h}$ increase or decrease according to the sign of $t_1 t_2$, but in such a way that

$$C\tilde{e} - \tilde{h} = C\tilde{e}_0 - \tilde{h}_0 \tag{15}$$

remains constant, where

$$C\tilde{e}_0 - \tilde{h}_0 = \frac{1}{\Omega_0^2}\left\{\frac{A t_2^2}{C-A} + \frac{B}{C-B} t_1^2\right\} \tag{16}$$

- As long as most of the kinetic energy is carried by the initial axis of rotation, we can approximate $\tilde{e} \approx \frac{1}{2} C\Omega^2$, and substituting this result in Equation (13) we obtain

$$\Omega\dot{\Omega}C = \frac{t_1 t_2}{\Omega} \frac{B-A}{(C-A)(C-B)} \tag{17}$$

where $\dot{\Omega}$ is the averaged change in ω_3. Equation (17) is easily integrated by separation of variables:

$$\Omega^3 - \Omega_0^3 = \frac{3 t_1 t_2}{C} \frac{B-A}{(C-A)(C-B)} (t - t_0) \tag{18}$$

or

$$\boxed{\Omega(t) = \Omega_0 \sqrt[3]{1 + \frac{(t-t_0)}{\tau}}} \tag{19}$$

with

$$\tau = \frac{C}{3 t_1 t_2} \frac{(C-A)(C-B)}{B-A} \Omega_0^3 \tag{20}$$

Another derivation of Equation (19) relies on use of the third Euler equation of Equation (1), where for the product $\omega_1 \omega_2$ the mean value obtained from Equation (3) is used. The mean value happens to be the product $\bar{\omega}_1 \cdot \bar{\omega}_2$. The result is identical to Equation (17), but the underlying assumptions are not so explicit. This approach will be employed for the extension to the rigid body with cables.

Returning to Equations (19) and (20) we can observe the following:

- $t_1 \cdot t_2 > 0$ implies that $\tau > 0$ and that Ω, $\tilde{e}$ and $\tilde{h}$ increase. The average spin increases, but slower and slower as time goes on. The time needed to double the initial spin rate is 7τ. The assumptions under which Equations (17) and (19) are derived remain satisfied. The limiting motion is a pure spin of infinite magnitude about the initial spin axis. This type of motion is also an equilibrium solution of Equation (1). Such motion is not possible for a finite value of ω_3.
- $t_1 t_2 < 0$ implies $\tau < 0$ and Ω, $\tilde{e}$ and $\tilde{h}$ decrease. While Ω decreases, the instantaneous mid-point of the ellipse moves away from the origin, and the nutational motion increases. When Ω approaches zero, the assumptions under which Equation (19) is derived become invalid. However, due to the one-third power law (compare with Fig. 4), Ω hardly changes at the beginning and then decreases to zero rather abruptly. Due to this fact, the predicted time τ to reach zero spin for the average ω_3 is better than one might expect a priori.

Finally, one can note that a reversal of the thrust direction does not affect the conclusions for spin-up or spin-down (assuming $\Omega_0 > 0$) as the sign of $t_1 t_2$ is conserved under such a transformation. This feature was confirmed by the simulations.

Rigid body appended symmetrically with two cable booms

The simulation results (Fig. 4) indicated that the structure of Equation (19) was conserved when the rigid body was appended with two symmetrically attached wires, on the intermediate principal axis and in the vicinity of the centre of mass of the central body. However, the destabilisation times obtained by using the central-body inertias in Equation (20) were much too short, whereas those obtained by using the rigidified total system inertias were much too long. Therefore, the linearised Euler equations for the system considered were taken from Reference 7. The ω_1, ω_2 equations are coupled with the meridian antisymmetric oscillations θ_{M1}. This set of three equations (21) is the equivalent of the first two of Equations (2). With the Laplace variable s, it becomes

$$\begin{vmatrix} A\,s & (C-B)\,\Omega & -2m_l\,a\,a+l\,\Omega^2 \\ -(C-A)\,\Omega & B\,s & 0 \\ s & \Omega & \dfrac{s^2}{1+\varepsilon}+\Omega^2 \end{vmatrix} \begin{vmatrix} \omega_1(s) \\ \omega_2(s) \\ \theta_{M1}(s) \end{vmatrix} = \begin{vmatrix} t_1\,s \\ t_2\,s \\ 0 \end{vmatrix} \qquad (21)$$

where

a = distance of the attachment point from the spin axis
l = equivalent length of the cable booms
m_l = equivalent tip-mass
ε = $a\,l$
A, B, C = central body inertias, as before.

The determinant of the matrix of Equation (21) gives the meridian-antisymmetric and nutation frequency. The solutions $\omega_1(s)$, $\omega_2(s)$, $\theta_{M1}(s)$ of Equation (21) are the Laplace-transformed time responses to continuous axial thrusting with zero initial conditions. We are only interested in the constant term of this solution. This is given by the residue corresponding to the pole $s=0$. After some elementary calculations,

$$\bar{\omega}_1 = \frac{-t_2}{\Omega\,(C-A)} \qquad (22)$$

$$\bar{\omega}_2 = \frac{t_1}{\Omega\,(C-B')} \qquad (23)$$

where $B' = B - 2m_l\,a(a+l)$

Equations (22) and (23) are identical to (4) and (5), except for the change from B to B'.

The equivalents of the third Euler equation are the two coupled equations for ω_3 and the equatorial-antisymmetric oscillations ψ_{L1}:

$$C\,\dot{\omega}_3 = -2m_l\,(1+\varepsilon)\,\Omega^2\,a\,l\,\psi_{L1} \qquad (24)$$

$$\ddot{\psi}_{L1} + \Omega^2\,\varepsilon\,\psi_{L1} = (1+\varepsilon)\,\dot{\omega}_3 \qquad (25)$$

As these equations will only be used for the average evolution of ω_3, we neglect the superimposed oscillations of ψ_{L1}. This is done by eliminating ψ_{L1} between Equations (24) and (25) after putting $\ddot{\psi}_{L1} \approx 0$. The result is

$$\dot{\omega}_3 \left[C + 2m_t (a+l)^2 \right] + (B - A)\,\omega_1 \cdot \omega_2 = 0 \tag{26}$$

where the dominant nonlinear term has been added. The coefficient C' of $\dot{\omega}_3$ is the total system inertia around the initial spin axis. Substitution of Equations (22) and (23) in (26) gives the equivalent of Equation (17):

$$\Omega^2 \dot{\Omega} = \frac{t_1 t_2 (B - A)}{C' (C - A)(C - B')} \tag{27}$$

Integration of Equation (27) gives the same result as (19) and the new expression for the destabilisation time is

$$\tau = \frac{C' (C - A)(C - B')}{3 t_1 t_2 (B - A)} \Omega_0^3 \tag{28}$$

The structure of Equation (28) is identical to that of Equation (20), but it contains a mixture of central-body inertias, system inertias and cable parameters.

Comparison of average spin-rate variations

The following data, extracted from Table 1, are used in Equations (28) and (19) to calculate the destabilisation times and final spin rates for the manoeuvres mentioned in the previous section:

$A = 78.37\,(\mathrm{kgm^2})$	$B = 163.51\,(\mathrm{kgm^2})$	$C = 170.98\,\mathrm{kgm^2}$
$t_1 = 3.26215\,(\mathrm{Nm})$	$t_2 = -3.8877\,(\mathrm{Nm})$	$l = 13.412\,(\mathrm{m})$
$a = 1.1\,\mathrm{m}$	$m_t = 0.560\,\mathrm{kg}$	
$B' = 145.631\,(\mathrm{kgm^2})$	$C' = 406.86$	

The equivalent length l is obtained by identifying the inertia about the Z-axis of the cable booms under mass conservation.

Table 3

Manoeuvre duration (s)	Initial spin (rpm)	Final spin measured (rpm)	Destabilisation time from (28) (s)	Final spin predictions from (19) (rpm)
82	10.97	10.36	447 = 7'27"	10.25
181	11.00	9.53	451 = 7'31"	9.27

Table 3 gives the destabilisation time τ for the two manoeuvres and the results for the spin rate. The order of magnitude of the latter is correct. The difference is probably caused by the fact that only one nonlinear term is used to construct Equation (26). As shown in Reference 11, a whole series of second-order terms comes in when the equations are developed to second order, and at the same time the vertical offset between the attachment points and the centre of mass is considered.

By inverting Equation (19) one can calculate a destabilisation time τ_m from the observed spin rates Ω_f and the manoeuvre duration t_{man}:

$$\tau_m = \frac{t_{man}}{(\Omega_f / \Omega_0)^3 - 1} \tag{29}$$

We obtain $\tau_1 = 8'39.93''$ and $\tau_2 = 8'37.56''$. The consistency of these results validates the structure of the expression used.

Conclusions

The many flight manoeuvres performed with Geos-1 and 2 have inspired great confidence in the stability of this type of satellite. The lesson taught by the analysis that has been presented here is that such extensive experience cannot guarantee the safety of a new type of manoeuvre.

The nonlinear nature of the effect stresses the importance of working on the complete equations of motion, at the cost of a discretisation procedure (multi-body approach). This approach complements the other alternative of keeping the flexible parts as a continuum and linearising the equations of motion.

Continuous axial thrusting causes large spin variations if the thruster is not located on a principal axis. A thruster located in the first or third quadrant causes a spin-down; a thruster located in the second or fourth quadrants causes a spin-up. The spin-down occurs much faster than the spin-up. The rate of spin variation is inversely proportional to the square of the initial spin. Given sufficient time, the spin becomes infinite and perpendicular to the torque direction, which is contrary to what one would expect intuitively.

References

1. Likins P 1976, *Interaction problems between the dynamics and control system for non-rigid spacecraft*, ESA SP-117
2. Boland Ph 1977, *Geos dynamic behaviour during manoeuvring Multibody approach*, ESA EWP 1064
3. Boland Ph, Janssens F 1979, *Theoretical predictions for Geos-1 dynamic experiment*, ESA EWP 1194
4. Wimmer W 1979, *Geos-1 FOP for dynamic experiment*, ESOC Geos Flight Operations Plan
5. Boland Ph 1978, *Spin rate variations of an asymmetric spinning body submitted to axial forces*, ESA EWP 1063
6. Magnus K 1971, *Kreisel-Theorie und Anwendungen*, Springer-Verlag (pp 143-155)
7. Janssens F 1976, *Dynamics of spinning satellites modelled as a rigid central body and spherical pendula as appendages*, ESA SP-117
8. Grammel R 1953, Die Stationären bewegungen des selbsterregten Kreisels und ihre Stabilität, *Ingenieur Archiv XXI*, 3
9. Grammel R 1954, Der selbsterregte unsymmetrische Kreisel, *Ingenieur Archiv XXII*, 2
10. Kluiters M A M 1966, Flat spin recovery of a spinning satellite, *AIAA Guidance and Control Conference*, San Diego
11. Janssens K 1975, *Some elementary considerations about the motion of long cable booms of a spinning satellite - Part 2*, ESOC Orbit and Attitude Department Working Paper 37

Manuscript received 14 November 1979